Published in IEEE JOURNAL OF OCEANIC ENGINEERING, VOL. 25, NO. 2, APRIL 2000, pp. 227-240

Modeling and Identification of Open-Frame Variable Configuration Unmanned Underwater Vehicles

Massimo Caccia, *Member, IEEE*, Giovanni Indiveri, and Gianmarco Veruggio

***Abstract*—A lumped parameter model of open-frame unmanned underwater vehicles (UUV's) including the effects of propeller–hull and propeller–propeller interactions is presented. The identification of the model parameters consists of a least squares method using only on-board sensor data without requiring any towing tank tests. The identification scheme is based on separate tests for the estimation of drag and thruster installation coefficients, taking into account propeller–hull and propeller–propeller effects first and inertia parameters subsequently. The scheme has been experimentally implemented on ROMEO, the latest UUV developed by CNR-IAN. Experimental results show both the effectiveness of the proposed method and the relevance of the propeller–hull and propeller–propeller interactions that are usually neglected in standard UUV models.**

***Index Terms*—Identification, modeling, unmanned underwater vehicles.**

NOMENCLATURE

$M \in \Re^{6\times6}$	Inertia matrix.
$M_A \in \Re^{6\times6}$	"Added mass" inertia matrix.
$C \in \Re^{6\times6}$	Coriolis and centripetal matrix.
$C_A \in \Re^{6\times6}$	"Added mass" Coriolis and centripetal matrix.
$D_L \in \Re^{6\times6}$	Linear drag matrix.
$D_Q \in \Re^{6\times6}$	Quadratic drag matrix.
$\underline{v}_{\rm rel}$	$= [u, v, w, p, q, r]^T \in \Re^{6\times1}$: surge, sway, heave, roll, pitch, and yaw velocities.
$F \in \Re^{6\times1}$	Nominal applied force.
$T \in \Re^{6\times1}$	Nominal applied torque.
$m_\xi \in \Re$	Inertia relative to the degree of freedom ξ including added mass effects.
$k_\xi \in \Re$	Linear drag coefficient relative to the degree of freedom ξ.
$k_{\xi\|\xi\|} \in \Re$	Quadratic drag coefficient relative to the degree of freedom ξ.
$\phi^n_\xi \in \Re$	Nominal applied force (torque) relative to the degree of freedom ξ.
$v_\xi \in \Re$	Additive noise relative to the degree of freedom ξ.
$V \in \Re$	Applied thruster voltage.
$n \in \Re$	Propeller revolution rate.
$\mu \in N$	Thrust mapping mode index.
$n_\xi(\mu) \in \Re$	Nondimensional thruster installation coefficient.

Manuscript received February 20, 1999; revised October 7, 1999. This work was supported in part by the Commission of the European Union under Contract MAS3-CT97-0083 (Project ARAMIS) and by PNRA (Programma Nazionale di Ricerche in Antartide), Task 4a-Robotica e Telescienza in Ambiente Estremo.

M. Caccia and G. Veruggio are with Consiglio Nazionale delle Ricerche, Istituto per l'Automazione Navale, 16149 Genova, Italy.

G. Indiveri was with Consiglio Nazionale delle Ricerche, Istituto per l'Automazione Navale, 16149 Genova, Italy, and with DIST, Department of Communications, Computer and System Science, University of Genova, 16145 Genova, Italy. He is now with the GMD-AiS, German National Research Center on Information Technologies, Institute for Autonomous Intelligent Systems, 53754 St. Augustin, Germany.

I. INTRODUCTION

IN THE LAST few years, after the satisfactory experiences of Jason [1] and Ventana [2], the employment of remotely operated vehicles (ROV's) for marine science applications has definitely grown. Among the many different kinds of unmanned underwater vehicles (UUV's), a new generation of ROV's with an interchangeable toolsled for different payloads has been developed. Examples of such systems are the deep-water vehicles Tiburon [3], [4] and Victor 6000 [5], [6] and the mid-water vehicle ROMEO [7], which are being exploited in a number of scientific programs [8], [9]. Many of these programs require high-precision maneuvering in the proximity of environmental structures, which cannot be altered by the vehicle movements (e.g., benthic applications for studying the sediment–water interface or visual inspection). Indeed, regardless of the specific mission requirements, the problem of designing motion controllers for underwater vehicles able to guarantee high-performance in terms of precision, agility, and optimization of the thruster action (i.e., reduction of power consumption and environment perturbations) has been extensively treated in literature.

Many different control methodologies ranging from sliding mode [10], [11] to H_∞ [12], [13] and adaptive techniques [14], [15] have been proposed to handle the uncertainties related to the knowledge of the hydrodynamic derivatives and the external disturbances. Whatever the control strategy to face parametric and environmental uncertainty is, a nominal vehicle model and an estimate of the dynamic equation parameters are necessary for both control and state estimation purposes. Notice that underwater vehicle linear speeds are usually obtained by model-based state estimation through noisy position measurements [15] or by noisy and biased low sampling rate direct measurements, as when Doppler velocimeters are used. In this framework, the need for performance improvements in navigation, guidance, and control, required to execute tasks such as high-precision hovering in the proximity of the seabed, motivates a deeper investigation on the methodologies for hydrodynamic modeling and identification of open-frame ROV's.

Conventional hydrodynamic derivative identification methods involve towing tank trials of the vehicle itself [16] or of a scaled model of the vehicle [17], expecting, in this case, an error in the estimate of some of the parameters up to 50% [18]. These kind of tests allow a complete model identification, but are lengthy, complex, and expensive. As a consequence, on-board sensor-based identification of a simplified model is to be preferred for variable-configuration vehicles as it can be simply and cheaply repeated when a significant variation in the systems structure occurs. Indeed, system identification as opposed to towing tank techniques for marine systems parameters identification has been proposed by several authors. As far as surface vessels are concerned, the use of extended Kalman filters (EKF's) has been first suggested and experimented by Abkowitz [19]. A state-augmentation version of an EKF for ship hydrodynamic coefficients identification has been proposed by Liu [20] and the tuning of ship models based on least squares (LS) and EKF to improve performance of dynamic positioning systems has been addressed by Selkäinaho [21] and Fossen *et al.* [22]. As far as underwater vehicles are concerned, system identification methodologies have been suggested by Goheen and Jefferys [23]. EKF-based identification of the surge motion of the NPS Phoenix autonomous underwater vehicle (AUV) has been presented by Marco *et al.* [24] while a LS identification approach for the IFREMER VORTEX vehicle is described by Ziani-Cherif *et al.* [25]. A combined use of LS and EKF methods for the identification of a ROV has been described by Alessandri *et al.* in [26]. Morrison and Yoerger [27] applied to the ROV Hylas a one-dimensional (1-D) system identification procedure based on numerical minimization of the error between the trajectories of the vehicle and several models during a free decay.

In the following, a research study focusing on the development of a procedure for the modeling and LS identification of an open-frame variable configuration ROV using on-board sensor data without requiring any towing tank tests, i.e., remarkably reducing costs, is presented [28]. A suitable lumped parameter model for thruster installation effects [29] has been defined and the thrusters installation coefficients, which take into account the propeller–hull and propeller–propeller interactions, have been estimated. Persistently exciting input signals have been designed considering the model structure, actuator dynamics, and type of available sensors. The LS identification procedure consists of two steps: 1) the drag coefficients are estimated by constant speed tests and 2) on the basis of their values a suboptimal sinusoidal input is designed to identify the inertia parameters.

The proposed methodology has been applied to model and identify ROMEO, the prototype ROV developed by CNR-IAN for robotics research and scientific applications.

The paper is organized as follows. Section II discusses the modeling of ROV dynamics and of the thruster installation coefficients. The LS-based identification procedure is reported in Section III. Experimental results obtained by adapting this procedure to the identification of the ROMEO vehicle are outlined in Section IV where general implementation issues are also discussed. Finally, Section V ends with some concluding remarks.

II. Modeling

A. Vehicle Modeling

The dynamic model of a UUV can be derived from the general Newton–Euler motion equation of a rigid body in a fluid medium. If the fluid is irrotational, inviscid, of uniform and constant density, and of infinite extent except for the rigid body itself [14], [30], [31], then the equation of motion can be expressed in spatial notation in the local reference frame as

$$\begin{aligned} &M\dot{\underline{v}}_{\mathrm{rel}} + C\left(\underline{v}_{2\mathrm{rel}}\right)\underline{v}_{\mathrm{rel}} \\ &\quad = -M_A\dot{\underline{v}}_{\mathrm{rel}} - C_A\left(\underline{v}_{1\mathrm{rel}}, \underline{v}_{2\mathrm{rel}}\right)\underline{v}_{\mathrm{rel}} - D_L\underline{v}_{\mathrm{rel}} \\ &\quad - D_Q\left|\underline{v}_{\mathrm{rel}}\right|\underline{v}_{\mathrm{rel}} + gW\left[\underline{k}_0^T, \underline{k}_0^T\right]^T + \left[\underline{F}^T, \underline{T}^T\right]^T \end{aligned} \quad (1)$$

where $\underline{v}_{\mathrm{rel}} = [\underline{v}_{1\mathrm{rel}}^T, \underline{v}_{2\mathrm{rel}}^T]^T = [u, v, w, p, q, r]^T$ is the six-dimensional speed column vector relative to the fluid, M is the 6×6 inertia matrix, $C(\underline{v}_{2\mathrm{rel}})$ is the Coriolis and centripetal matrix, M_A and $C_A(\underline{v}_{1\mathrm{rel}}, \underline{v}_{2\mathrm{rel}})$ are the added mass and added mass Coriolis-like matrices, D_L and D_Q are the linear and quadratic drag matrices, W is the weight and buoyancy matrix ($g = 9.81$ m/s^2 is the gravity acceleration), k_0 is the projection of the z-axis global inertial reference frame unit vector on the local body fixed reference, and $[F^T, T^T]^T$ are the force and torque produced by the vehicle's propulsion system. In the following, all the quantities considered up to now will be assumed as projected on the local body fixed reference frame.

The experimental identification of a complete ROV model such as the one given by (1) is not feasible with only standard on-board sensors because it would require a complete state knowledge. Indeed, it may be performed with complex and expensive towing tank facilities as described by Nomoto *et al.* [17] or Goheen [16], but such an approach is not indicated for systems having a variable and mission-dependent configuration. Moreover, in many standard maneuvering conditions, e.g., plane surge motion or vertical translation, and generally at low operating speeds, the coupling terms may be reasonably neglected without serious loss of information. As a consequence, on-board sensor-based identification experiments usually refer to a simplified uncoupled model that can be deduced from (1) neglecting the off-diagonal elements of the added mass matrix, the Coriolis and centripetal kinematics, and drag coupling terms. This approximation relies on the fact that: 1) the off-diagonal elements of the added mass matrix of a rigid body having three symmetry planes are identically null [30]; 2) the off-diagonal elements of the positive definite matrix are much smaller than their diagonal counterparts [31]; and 3) the hydrodynamic damping coupling is negligible at low speeds. The resulting model structure for a single degree of freedom is

$$m_\xi\dot{\xi} = -k_\xi\xi - k_{\xi|\xi|}\xi\left|\xi\right| + \phi_\xi + \nu_\xi \quad (2)$$

where m_ξ is the inertia relative to the considered degree of freedom, ξ is the 1-D velocity, k_ξ and $k_{\xi|\xi|}$ are the linear and quadratic drag coefficients, ϕ_ξ is the applied force or torque, and ν_ξ is the disturbance modeling otherwise unmodeled phenomena as cable effects. This kind of uncoupled model structure is certainly the most common in the literature of underwater vehicles regarding guidance, navigation, and control schemes

[24], [25]. Parameters are estimated assuming the nominal actuator action ϕ_ξ known. The knowledge of ϕ_ξ is actually related to the fact that the relation between applied thruster voltage and torque has been identified *a priori* for each single thruster in a thrust tunnel. A potentially serious drawback of such methods is related to the fact that the identified thruster model neglects the propeller–propeller and/or propeller–hull interactions that occur in the vehicle under the operating conditions. Propeller–hull interactions are a well-known and studied phenomenon in surface vessels [30], however, as far as UUV's are concerned, they have seldom been taken into account. To the knowledge of the authors, only Goheen and Jefferys [29] model explicitly such interactions although without measuring directly the coefficient's values; in their words, "the installation coefficients of a thruster take into account the differences in force that the thruster provides when operating in the proximity of the ROV, as opposed to when it is tested in open water." In the following, these phenomena have been modeled introducing the thruster installation coefficient η_ξ, which takes account the aggregate reduction in the efficiency of the thrusters applying the desired 1-D force/torque, obtaining the 1-D model

$$m_\xi \dot{\xi} = -k_\xi \xi - k_{\xi|\xi|} \xi \, |\xi| + \eta_\xi \phi_\xi^n + \nu_\xi. \tag{3}$$

The nominal actuator action ϕ_ξ^n is assumed to be known, i.e., computed according to a thrust tunnel identified model. The inertia and drag coefficients are assumed to be independent from how the total thrust is distributed on the vehicle's thrusters (thrust mapping μ), while the installation coefficient is definitely expected to depend on μ, i.e., $\eta_\xi = \eta_\xi(\mu)$. The model given by (3) can be identified by following two different approaches. Either (3) is divided by the non-null $\eta_\xi(\mu)$ giving rise to a model in which each parameter depends on the thrust mapping in an *a priori* unpredictable fashion

$$\frac{m_\xi}{\eta_\xi(\mu)} \dot{\xi} = -\frac{k_\xi}{\eta_\xi(\mu)} \xi - \frac{k_{\xi|\xi|}}{\eta_\xi(\mu)} \xi \, |\xi| + \phi_\xi^n + \frac{\nu_\xi}{\eta_\xi(\mu)} \tag{4}$$

or the parameter vector $\theta = [m_\xi k_\xi k_{\xi|\xi|} \eta_\xi(\mu) \nu_\xi]^T$ is identified for each mapping μ, of interest being the dependence on μ embedded in the only $\eta_\xi(\mu)$ rather than in each parameter. Notice that the external disturbance ν_ξ is not necessarily zero mean; thus, its mean value must be identified. As (3) is homogeneous in θ, in order to implement this second, more appealing approach, $\eta_\xi(\mu)$ must be known for at least one mapping μ. Generally, it is not difficult to heuristically find a specific thrust mapping $\mu*$ for which $\eta_\xi(\mu*)$ can be reasonably thought to be 1, i.e., a mapping in which thrusters operate in open water as during the thrust tunnel identification experiments.

B. Thruster Modeling

The modeling and control of underwater vehicle thruster systems have received wide attention in the literature in the last years [32]–[35].

In many applications, the servo velocity loop of the controlled thruster system has a negligible time constant with respect to the overall vehicle's time constant [36], and thus the thruster dynamics can be neglected with respect to the vehicle's dynamics. In this hypothesis, the propeller thrust is modeled as

$$\tau = c_\tau n|n| - c_s|n|v_a \tag{5}$$

where v_a is the velocity of the fluid through the propeller blade (velocity of advance) and $-c_s|n|v_a$ is a saturation term [31]. By virtue of the creeping motion of UUV's, the saturation term can be neglected in many standard operational conditions as widely accepted in the literature [14], [17], [25], [31], [32]. Moreover, under steady-state conditions, the neglected thrust drag term $\tau = -c_s|n|v_a$ will be indirectly taken into account by the drag forces considered in the equation of motion (3) of the vehicle. Thus, neglecting the motor dynamics, the thruster force may be modeled as

$$\tau = c_V V \, |V| \tag{6}$$

where c_V is an unknown constant and V is the control voltage, which is applied to the thruster servo-amplifiers. Since the thruster time constant has been neglected with respect to the overall vehicles one, V is assumed to be simply proportional to the propeller revolution rate. It is worth noting that, neglecting the velocity of advance, (6) is expected to be more accurate farther from the propeller revolution rate inversion points. In particular, high-frequency sign changes of n that may occur with pseudorandom binary inputs typical of identification experiments produce unmodeled turbulence next to the thrusters, making the output thrust computed by the standard model less accurate. In the following, the nominal actuator action ϕ_ξ^n will be assumed to be computed on the basis of (6) having been c_V estimated by thrust tunnel experiments.

III. Identification

The structure of (3) is well suited for the separate identification of the drag and inertia parameters when particular static or dynamic conditions are met. In particular, the drag and thruster installation coefficients can be estimated by a standard LS procedure on the basis of the estimated velocity under different steady-state (constant velocity) conditions. The constant regime velocity corresponding to the different constant applied thrusts may be accurately estimated by LS with only position measurements. The experiments described in the following show that, even when only low sampling frequency position measurements are available (e.g., 3-Hz sampling frequency sonar profilers), the estimated velocity standard deviation is lower than 3% of the velocity. Once the drag parameters have been determined, a suboptimal sinusoidal force/torque input is designed in order to identify the vehicle inertia. Such input guarantees observability [37] and minimizes the turbulence generated next to the propellers.

A. Identification of the Drag and Thruster Installation Coefficients

Under steady-state conditions, i.e., when the applied force/torque is constant, (3) becomes

$$0 = -k_\xi \xi - k_{\xi|\xi|} \xi \, |\xi| + \eta_\xi \phi_\xi^n + \nu_\xi \tag{7}$$

where the unknown parameters are the linear and quadratic drag coefficients, the thruster installation coefficient, and the mean value of the external disturbances. As long as a reliable estimate of the velocity is available corresponding to different values of the applied nominal thrust, these parameters can be estimated by a standard LS technique. A set of n^* constant force/torque ϕ^*_ξ inputs are applied to the vehicle with a specific thrust mapping mode in which thrusters are assumed to operate in open water, i.e., $\eta^*_\xi = 1$. Furthermore, M sets of $n(\mu)$ constant nominal inputs

$$\left(\phi^n_{\xi_1}(\mu), \cdots, \phi^n_{\xi_{n(\mu)}}(\mu)\right)\Big|_{\mu=1}, \quad \cdots, \left(\phi^n_{\xi_1}(\mu), \cdots, \phi^n_{\xi_{n(\mu)}}(\mu)\right)\Big|_{\mu=M}$$

corresponding to $\mu = 1, \cdots, M$ propulsion mappings having different propeller–propeller and propeller–hull interactions can be applied.

As the velocity and nominal force are known, (7) can be written in regression form $y = H\theta$ as shown in (8)–(10), shown at the bottom of the page, where $\overline{\nu}$ represents the mean value of the external forces acting on the vehicle and $\eta_\xi(\mu)$ with μ ranging from 1 to M are the thruster installation coefficients corresponding to the M different thrust mapping modes.

According to LS theory, the standard deviation $\hat{\sigma}_\theta$ of the estimated parameter $\hat{\theta} = (H^T H)^{-1} H^T y$ is computed as

$$\hat{\sigma}_\theta = \sqrt{\mathrm{diag}\left((H^T H)^{-1}\sigma^2_\varepsilon\right)} \tag{11}$$

where σ^2_ε is the Gaussian zero mean measurement noise variance. As suggested in [37], if such variance is unknown, it can be estimated by

$$\hat{\sigma}^2_\varepsilon = \frac{\left(y - H\hat{\theta}\right)^T \left(y - H\hat{\theta}\right)}{\dim(y) - \dim(\theta)}. \tag{12}$$

In the remainer of the paper, the quantity $100(\hat{\sigma}_\theta/|\hat{\theta}|)$ will be referred to as the percentile parameter error.

B. Identification of the Inertia Coefficients

Having identified the drag parameters as described above, the basic idea is to consider them to be known and use this knowledge to design a suboptimal experiment for the identification of the inertial quantities. The model to identify is given by (3) where the drag and thruster efficiency coefficients are assumed known from the identification experiments described above.

The design of the inertia parameter identification experiment has to take into account some important constraints: i) in the absence of accelerometers the identification process must be performed with the only velocity and position measurements and applied force estimate and ii) since the adopted propulsion model is known to be very accurate when the propellers do not suddenly change revolution direction, thus the sign of ϕ^n_ξ has to be kept constant during the whole experiment.

$$y = \left[\phi^*_{\xi_1} \quad \cdots \quad \phi^*_{\xi_{n^*}} \quad 0 \quad \cdots \quad \cdots \quad \cdots \quad 0\right]^T, \qquad y \in \Re^{n^* + \sum_{\mu=1}^{M} n(mu),\, 1} \tag{8}$$

$$H = \begin{bmatrix} \xi^*_1 & \xi^*_1|\xi^*_1| & -1 & 0 & \cdots & \cdots & 0 \\ \vdots & \vdots & \vdots & \vdots & \vdots & \vdots & \vdots \\ \xi^*_{n*} & \xi^*_{n*}|\xi^*_{n*}| & -1 & 0 & \cdots & \cdots & 0 \\ \xi_1|_{\mu=1} & \xi_1|\xi_1||_{\mu=1} & -1 & -\phi^n_{\xi_1}(\mu)\Big|_{\mu=1} & 0 & \cdots & 0 \\ \vdots & \vdots & \vdots & \vdots & \vdots & \vdots & \vdots \\ \xi_{n(\mu)}\big|_{\mu=1} & \xi_{n(\mu)}\left|\xi_{n(\mu)}\right|\big|_{\mu=1} & -1 & -\phi^n_{\xi_{n(\mu)}}(\mu)\Big|_{\mu=1} & 0 & \cdots & 0 \\ \vdots & \vdots & \vdots & \vdots & \vdots & \vdots & \vdots \\ \xi_1|_{\mu=M} & \xi_1|\xi_1||_{\mu=M} & -1 & 0 & \cdots & 0 & -\phi^n_{\xi_1}(\mu)\Big|_{\mu=M} \\ \vdots & \vdots & \vdots & \vdots & \vdots & \vdots & \vdots \\ \xi_{n(\mu)}\big|_{\mu=M} & \xi_{n(\mu)}\left|\xi_{n(\mu)}\right|\big|_{\mu=M} & -1 & 0 & \cdots & 0 & -\phi^n_{\xi_{n(\mu)}}(\mu)\Big|_{\mu=M} \end{bmatrix}, \quad H \in \Re^{n^* + \sum_{\mu=1}^{M} n(\mu), 3+M} \tag{9}$$

$$\theta = \left[k_\xi \quad k_{\xi|\xi|} \quad \overline{\nu} \quad \eta_\xi(\mu)|_{\mu=1} \quad \cdots \quad \eta_\xi(\mu)|_{\mu=M}\right]^T, \qquad \theta \in \Re^{3+M,\,1} \tag{10}$$

Equation (3) can be linearized about the operating velocity ξ^* obtaining a linear model, which corresponds to a first order system with time constant

$$t_c = \frac{m_\xi}{k_L} \quad \text{where} \quad k_L = k_\xi + 2k_{\xi|\xi|}\,|\xi^*|\,. \tag{13}$$

Note that as m_ξ is the sum of inertia (known) and added inertia (always positive) and k_ξ, $k_{\xi|\xi|}$ and ξ^* are known, a lower bound of the time constant t_c is known. Moreover as added mass is expected to be at most 100% of the inertial mass, also an upper bound of t_c is given.

A common criterion [37], [38] for the choice of the inputs is to maximize the cost function $J = -\log\det M$, where M is the Fisher's information matrix which depends on the adopted inputs. In robotic applications, this criterion, named the d-optimal criterion, has been successfully adopted by Swevers *et al.* [39], [40] for the identification of an industrial arm. In particular, a first-order system can be optimally identified with a single sine input of frequency [37]

$$\omega_{opt} = \frac{1}{\sqrt{3}t_c}. \tag{14}$$

The input force for the inertia identification experiments is thus chosen to be of the form

$$\phi_\xi^n = \widehat{\phi}_\xi^n + \Delta\phi_\xi^n \sin(\omega_{\rm opt} t)\,. \tag{15}$$

$\widehat{\phi}_\xi^n$ and $\Delta\phi_\xi^n$ are selected so that the corresponding regime velocity ξ^* is in the standard operating range, and $\Delta\phi_\xi^n \le \widehat{\phi}_\xi^n$ in order to avoid force inversions. The d-optimal frequency $\omega_{\rm opt}$ is selected in accordance to (14). The system time constant t_c needed to compute $\omega_{\rm opt}$ is estimated *a priori* by (13) assuming m_ξ to be equal to the inertia in air $m_\xi^{\rm air}$ plus a term ranging from 10% to 100% of $m_\xi^{\rm air}$ that models added mass.

To cope with the absence of an acceleration measurement, (3) must be integrated, giving

$$\begin{aligned} &m_\xi\xi(t) - m_\xi\xi_0 - k_\xi\chi_0 - b_\xi t = y_\xi \\ &y_\xi \equiv \varphi_\xi(t) - k_\xi\chi(t) - k_{\xi|\xi|}I(t) \end{aligned} \tag{16}$$

where $\varphi_\xi(t) = \eta_\xi \int_0^t \phi_\xi^n(\varsigma)\,d\varsigma$, $\chi(t)$ is the position, $I(t) = \int_0^t \xi(\varsigma)|\xi(\varsigma)|\,d\varsigma$, and b_ξ is an eventual bias due to the mean of ν_ξ and to the numerical integrations performed to calculate C and I. Note that the integration process does not affect the d-optimal frequency choice as the integral of (3) has the same structure, in particular the same time constant. As the drag constants, velocity, and position are assumed to be known, (16) can be written in discrete-time regression form $y = H\theta$ as

$$y = \begin{bmatrix} \varphi_1 - k_\xi\chi_1 - k_{\xi|\xi|}I_1 \\ \vdots \\ \varphi_N - k_\xi\chi_N - k_{\xi|\xi|}I_N \end{bmatrix} \tag{17}$$

$$H = \begin{bmatrix} \xi_1 & -1 & -t_1 \\ \vdots & \vdots & \vdots \\ \xi_N & -1 & -t_N \end{bmatrix} \tag{18}$$

$$\theta = [\, m_\xi \quad m_\xi\xi_0 + k_\xi\chi_0 \quad b_\xi \,]^T \tag{19}$$

and N the number of samples.

Within this approach, the uncertainty of the inertia parameter estimate is expected to be at least of the same order of magnitude as the drag parameter uncertainty. As estimating the inertia m_ξ is somehow equivalent to estimating the time constant t_c of the linearized system, by standard error analysis it follows that $\delta t_c/t_c \cong \delta k_L/k_L$. Moreover, the nominal applied force ϕ_ξ^n, assumed to be perfectly known, will actually be affected by some error. Numerical errors will also be introduced into the computation of y given by (17) since, due to the eventual absence of a velocity measurement, the I_i, $i \in [1, N]$ are calculated filtering the acquired position signal with an off-line Savitzky–Golay polynomial filter [41] to evaluate the velocity ξ and then integrating numerically $\xi|\xi|$ over time. Numerical integrations must also be performed on the position signal and on the applied force in order to compute y. These considerations and the fact that the sampling rate of the position measurements is very low (e.g., 3.3 Hz for echo-sounders used for the surge and sway and 10 Hz for the yaw) suggest that the inertia parameter identification by only on-board position measurements cannot be expected to be very precise. Nevertheless, experiments have shown that, in the case of ROMEO, the estimated value is good enough to provide reliable and useful models for motion estimation and control purposes.

IV. Applications: ROMEO Modeling and Identification

The methodology for the identification of UUV's described in Section III has been tested on ROMEO, an over-actuated open-frame ROV developed by the CNR-IAN for robotics research and scientific applications.

A. ROMEO Mechanical Design and Thruster Configuration

ROMEO, which is about 1 m in height, 0.9 m in width, and 1.3 m in length, weighs about 450 kg in air and is intrinsically stable in pitch and roll. It is divided into three sections. A steel frame, which is 0.6 m in height, supports the two upper sections, constituted by foam for buoyancy and the electronics and propulsion systems. The bottom section of the vehicle consists of an interchangeable toolsled for scientific devices, which, in the standard version, is equipped with two cylindrical canisters for batteries and payload electronics (see Fig. 1). The overall structure of the vehicle is symmetric with respect to both the xz and yz planes, and the eight thrusters are arranged two by two in the corners, with the horizontal ones parallel to the diagonals of the xy section. This thruster configuration enables the full controllability of the vehicle's motion and the possibility of distributing the propulsion and control forces according to constraints of a different nature. Scientific applications can require a toolsled equipped with dedicated devices, as in the case shown in Fig. 2, where a "microness" (zooplankton sampler) is positioned in the middle. More detailed information about ROMEO's mechanical, computer, and software design can be found in [7].

B. Distribution of the Propulsion and Control Forces

The resultant force and torque exerted by the vehicle's actuators are computed as $\phi = B\tau$, where $B \in \Re^{m,n}$ is the control matrix, and τ, the vector of the actuator thrusts com

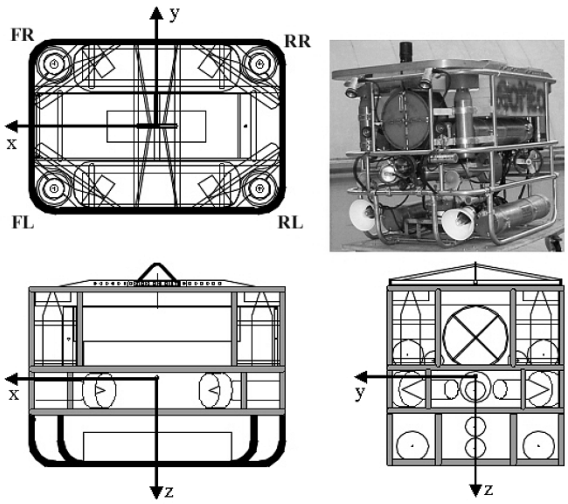

Fig. 1. Clockwise from the top right: top view of ROMEO in which the horizontal and vertical thrusters (labeled FR, FL, RR, RL as described in the text) and the principal canister are clearly visible; a picture (diagonal view) of the vehicle in its standard payload configuration; a lateral view of ROMEO; and a front view of ROMEO.

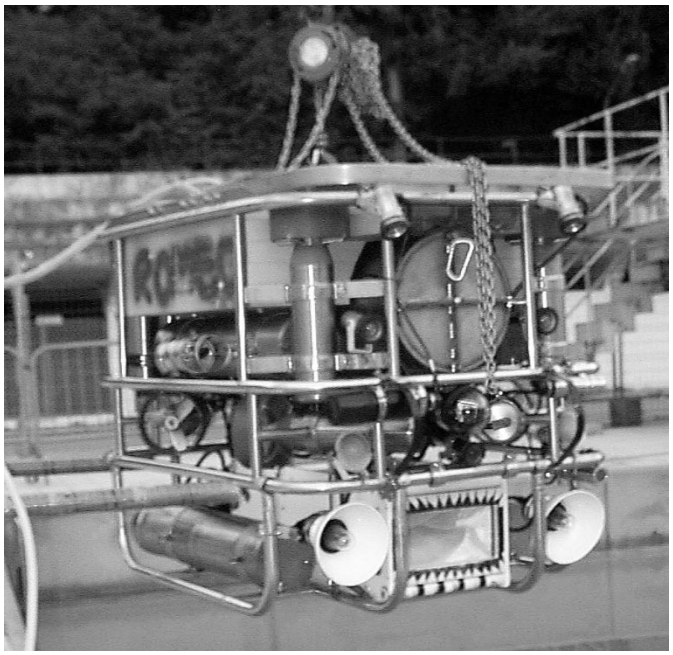

Fig. 2. ROMEO in plankton sampling payload configuration.

puted according to (6). In the case of over-actuated vehicles, B is non-square with $m < n$ and $\mathrm{rank}(B) = m$.

In the case of ROMEO, the horizontal control of surge, sway, and yaw is uncoupled from the vertical control of roll, pitch, and heave. Two control matrices

$$B_H = \begin{bmatrix} 1 & 1 & -1 & -1 \\ 1 & -1 & 1 & -1 \\ 1 & -1 & -1 & 1 \end{bmatrix}$$

and

$$B_V = \begin{bmatrix} -1 & 1 & -1 & 1 \\ -1 & -1 & 1 & 1 \\ 1 & 1 & 1 & 1 \end{bmatrix}$$

are defined such that $\phi_H = B_H \tau_H$ and $\phi_V = B_V \tau_V$, where $\tau_H = [\tau_{HFL} \quad \tau_{HFR} \quad \tau_{HRL} \quad \tau_{HRR}]^T$ and $\tau_V = [\tau_{VFL} \quad \tau_{VFR} \quad \tau_{VRL} \quad \tau_{VRR}]^T$ are the horizontal and vertical vectors of the actuator thrusts, and $\phi_H = [F_u/\cos\alpha \quad F_v/\sin\alpha \quad T_r/b]^T = [X \quad Y \quad N]^T$ and $\phi_V = [T_p/c \quad T_q/d \quad F_w]^T = [L \quad M \quad Z]^T$ are the normalized horizontal and vertical force-torque vectors. In the adopted notation, α is the module of the angle between the horizontal thrusters and the vehicle's longitudinal axis, while b, c, and d are the thruster arms with respect to the vehicle center of mass, respectively, for yaw, roll, and pitch motion. The subscripts H/V, F/R, and L/R stand for horizontal/vertical, front/rear, and left/right, respectively, indicating the thruster's position as shown in Fig. 1.

Since there are more control inputs than controllable degrees of freedom (DOF's), it is possible to find "optimal" distributions of the control actions with the constraint $\phi = B\tau$, satisfying some physical constraints or minimizing a particular cost function. This is, for instance, the case of the Moore–Penrose pseudo-inverse $B^{\#} = P^{-1}B^T(BP^{-1}B^T)^{-1}$, such that $\tau^{\#} = B^{\#}\phi$ minimizes the quadratic energy cost function $J = (1/2)\tau^T P \tau$ [31].

The possibility of mapping the control forces onto the actuator thrusts in different ways has been exploited in order to design and execute dedicated experiments for the identification of uncoupled hydrodynamics effects and of propeller interactions. Thus, a set of different distribution of the control forces has been defined as summarized in Table I. For each mapping mode, the motion direction where the propeller can be assumed to work in open water without remarkable interactions with the vehicle hull and other propellers is indicated, if existing.

C. Thruster Model Identification

Neglecting the motor dynamics, the thruster force τ can be modeled as a function of the control voltage applied to the thruster servo-amplifiers according to (6). In the case of ROMEO, the thruster model has been identified with a LS procedure putting the whole actuator (motor, propeller, and nozzle) in a thrust tunnel and measuring the force τ as a function of a set of input voltages V. The experimental relationship between the input voltage and thrust at bollard conditions is shown in Fig. 3. The thruster coefficient c_V of (6) has been identified to be $1.02(N/V^2)$ and $1.09(N/V^2)$ with a percentile error of 3.0% and 3.7% for positive and negative thrust, respectively.

D. Experimental Identification

The ROMEO's dynamics in the surge, heave, yaw, and sway DOF's have been modeled and experimentally identified. In all the experiments, the required velocities for all the DOF's have been estimated off-line on the basis of position measurements with a noncausal Savitzky–Golay polynomial filter [41] of fourth order with a symmetric moving window of different lengths according to the specific DOF.

Heave trials, performed under the Antarctica ice canopy in order to improve the vehicle's performances in executing under-ice scientific surveys [7], revealed the strong interactions between the vehicle's hull and the vertical propellers. The combined estimation of the heave linear and quadratic drag

TABLE I
THRUST MAPPING MODES

thrust mapping mode	criterion	thruster forces				motion direction with $\eta_\xi = 1$
vertical motion		τ_{VFL}	τ_{VFR}	τ_{VRL}	τ_{VRR}	
vertical all pitch, roll, heave	$\min J = \frac{1}{2}\tau_V^T\tau_V$	$\frac{-L-M+Z}{4}$	$\frac{L-M+Z}{4}$	$\frac{-L+M+Z}{4}$	$\frac{L+M+Z}{4}$	-
vertical all	$\min J = \frac{1}{2}\tau_V^T\tau_V$, $L=0$, $M=0$	$\frac{Z}{4}$	$\frac{Z}{4}$	$\frac{Z}{4}$	$\frac{Z}{4}$	downward heave
horizontal motion		τ_{HFL}	τ_{HFL}	τ_{HRL}	τ_{HRR}	
horizontal all	$\min J = \frac{1}{2}\tau_H^T\tau_H$	$\frac{X+Y+N}{4}$	$\frac{X-Y-N}{4}$	$\frac{-X+Y-N}{4}$	$\frac{-X-Y+N}{4}$	-
surge front	$\tau_{HRL}+\tau_{HRR}=0$, $Y=0$	$\frac{X}{2}+\frac{N}{4}$	$\frac{X}{2}-\frac{N}{4}$	$-\frac{N}{4}$	$\frac{N}{4}$	forward surge
surge rear	$\tau_{HFL}+\tau_{HFR}=0$, $Y=0$	$\frac{N}{4}$	$-\frac{N}{4}$	$-\frac{X}{2}-\frac{N}{4}$	$-\frac{X}{2}+\frac{N}{4}$	backward surge
sway left	$\tau_{FR}+\tau_{RR}=0$, $X=0$	$\frac{Y}{2}+\frac{N}{4}$	$-\frac{N}{4}$	$\frac{Y}{2}-\frac{N}{4}$	$\frac{N}{4}$	right sway
sway right	$\tau_{FL}+\tau_{RL}=0$, $X=0$	$\frac{N}{4}$	$-\frac{Y}{2}-\frac{N}{4}$	$-\frac{N}{4}$	$-\frac{Y}{2}+\frac{N}{4}$	left sway
yaw front-left rear-right	$\tau_{HFR}+\tau_{HRL}=0$, $X=0$, $Y=0$	$\frac{N}{2}$	0	0	$\frac{N}{2}$	clockwise yaw
yaw front-right rear-left	$\tau_{HFL}+\tau_{HRR}=0$, $X=0$, $Y=0$	0	$-\frac{N}{2}$	$-\frac{N}{2}$	0	counter-clockwise yaw

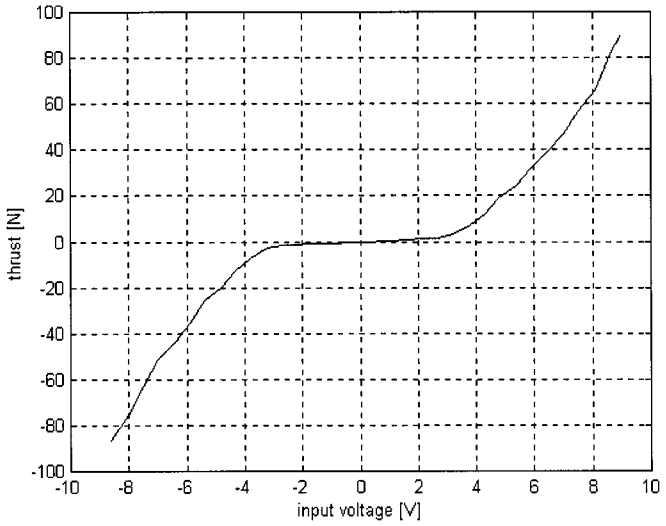

Fig. 3. Nominal thrust (N) versus applied voltage (V) according to the thrust tunnel data.

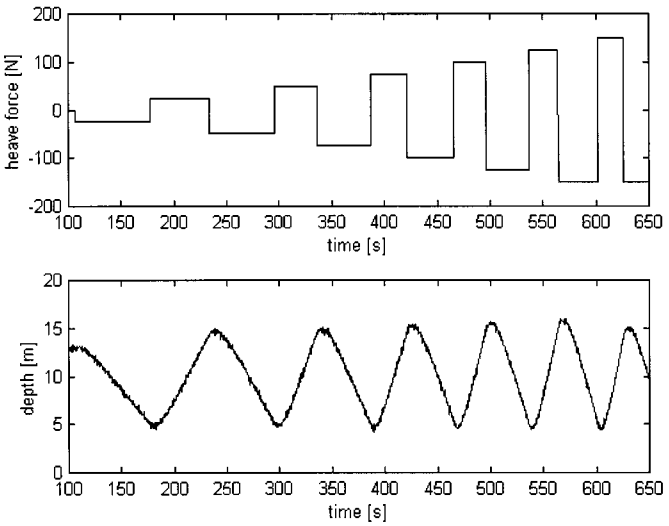

Fig. 4. Heave drag coefficients identification tests. Top: nominal applied heave thrust (N) versus time (s). Bottom: relative 10-HZ sampling rate measured depth (m) versus time (s).

coefficients, weight-buoyancy force, and thruster installation coefficient has been performed by processing data collected during up and down steady-state motions. Five different experiments, numbered 0–4, have been performed with inputs of the kind shown in Fig. 4 each with a different vehicle weight. During experiments 0 and 1, the vehicle was positive, during experiment 2 it was roughly neutral, and in the last two experiments it was negative. Weight was changed by adding on ROMEO's top, during each experiment, one diver's lead weight (about 0.7 kg in water) which reasonably does not affect the hydrodynamic derivatives but only the overall weight. The vehicle's depth was measured by a 10-Hz sampling rate depth-meter.

During all experiments, the heading of the vehicle was kept constant by the action of the heading autopilot. Nevertheless, as reported in [28] and [42], where different models of the vehicle's dynamics have been evaluated, the momentum drag in the vertical direction due to horizontal thrusters can be embedded in the standard linear heave drag term. According to

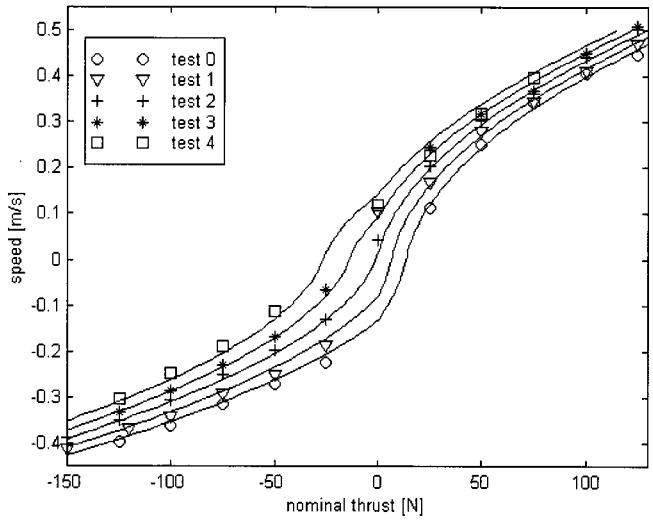

Fig. 5. LS estimated velocity (m/s) versus nominal applied thrust (N) in the heave direction for five different vehicle weights and relative identified models.

Section III-A, during the ith experiment, the vehicle's model in stationary conditions can be written as

$$k_w w + k_{w|w|} w|w| - \eta_w \phi_w^n - W - i\Delta W = 0,$$
$$i = 0, \cdots, 4 \quad \begin{cases} \eta_w = 1 \,\forall\, \phi_w^n \geq 0 \\ \eta_w < 1 \,\forall\, \phi_w^n < 0 \end{cases} \tag{20}$$

where

w heave velocity;
W weight-buoyancy force in experiment 0;
ΔW weight added to ROMEO in each experiment.

The parameter vector $[k_w \quad k_{w|w|} \quad W \quad \Delta W \quad \eta_w]^T$ has been identified with a standard LS procedure as shown in Section III-A. The results are reported in Table II. The measured and estimated relationships between the nominal thrust and the vehicle's heave velocity are shown in Fig. 5.

With reference to Table II, notice that, according to the above identified model (20) and in perfect accordance with the actual experimental setup, the estimated buoyancy force during experiments 0 and 1 points upwards, during experiment 2 is roughly null, and during experiments 3 and 4 points downwards. On the contrary, if the same data are processed assuming that the applied force is the nominal one in both the positive and negative directions, thus totally neglecting the propeller–hull interactions that occur during vertical surfacing motions, the results displayed in Fig. 6 are obtained [28], [42]. In order to compensate for the overestimated upward force due to the neglected propeller–hull interactions, weight is overestimated, always resulting in a value larger than the actual value.

It is worth noting that preliminary tests performed in a swimming pool revealed that the vertical thrusters behave as in a thrust tunnel (open water) when pushing down and with an efficiency reduction of about 40% when pulling up in static conditions. This value is almost equal to the identified value of 0.56 of the thruster's installation coefficient, reported in Table II. As shown in Figs. 7–10, ROMEO has been fixed to a load cell in a pool, and the maximum static heave force has been measured in both the positive and negative vertical directions.

Trials to identify the vehicle's model on the horizontal plane, i.e., the surge, sway, and yaw 1-D models, have been executed in a swimming pool. The vehicle's heading was measured at a 10-Hz sampling rate with a KVH-DGC100 compass. In order to reduce any possible interference with the deformations of the magnetic field induced by the reinforced concrete structure of the pool, the automatic compass calibration and compensation procedure has been executed and the vehicle's rotations at zero linear speed were performed in the middle of the pool. The position in the horizontal plane was measured with respect to the pool walls at a 3.33-Hz sampling rate by a couple of Tritech ST-200 echo-sounders mounted on the front and left sides of the vehicle. All the nominal thrusts have been estimated by the thrust-tunnel identified model described in Section IV-C.

During the identification tests of the yaw drag, the vehicle has been excited with torque input signals in a range of steady-state yaw rates between -20 and $+20$ deg/s as shown in Fig. 11. The vehicle worked in *yaw front-left rear-right* mapping mode in order to enable the thrusters to work in open water when positive torque was applied and with remarkable interactions with the hull in case of negative torque ($\eta_r^{\text{hull}} < 1$). In addition, tests performed in *horizontal all* mapping modes enabled the evaluation of $\eta_r^{\text{hull–propeller}}$, a second horizontal thruster installation coefficient that takes into account both the propeller hull and the propeller–propeller interactions occurring among horizontal thrusters on the same side of the vehicle. The estimated parameters $[k_r \quad k_{r|r|} \quad \eta_r^{\text{hull}} \quad \eta_r^{\text{hull–propeller}}]^T$ are reported in the upper section of Table III.

If only the steady-state yaw rates normally bounded at 10 deg/s are considered in order to identify the vehicle's yaw model under typical operating conditions, the results reported in the middle section of Table III are obtained. For a quantitative understanding of the reported data, notice that, if a process $y = H\theta + \varepsilon$ is normally distributed, so is the LS estimated parameter vector $\hat{\theta}_{\text{LS}} = H^T(H^T H)^{-1} y$, as linear functions of normal variables are normal themselves. This last property is very useful since, if the parameter vector $\hat{\theta}_{\text{LS}}$ is assumed to be normally distributed with known variance, then the standard Gaussian hypothesis testing technique [43] may be applied to the overfitting or model selection problem. Overfitting of the data by the model can be detected by evaluating the variance of the parameter's estimate. Roughly speaking, if the parameter's variance is too large, the parameter itself is said to be *statistically insignificant* and it might just as well be put to zero. More precisely, if the parameter's percentile error is larger than 51.02%, there is 95% confidence limit that the parameter is statistically insignificant, i.e., null.

On the basis of this result, the quadratic drag term in ROMEO's yaw model at low yaw rates, i.e., normally bounded at 10 deg/s, was negligible and a linear model has been identified estimating the parameter vector $[k_r \quad \eta_r^{\text{hull}} \quad \eta_r^{\text{hull–propeller}}]^T$ as reported in the lower section of Table III.

The estimated linear drag k_r, which includes all the drag effects, is higher than in the case of the linear and quadratic model, as well as the η_r^{hull} coefficient. Propeller–hull interactions seem to increase when higher propeller revolution rates are considered also.

TABLE II
ROMEO HEAVE MODEL: ESTIMATED DRAG, THRUSTER INSTALLATION COEFFICIENTS, AND WEIGHT-BOUYANCY FORCES

	k_w [Ns/m]	$k_{w\|w\|}$ [Ns^2/m^2]	W [N]	ΔW [N]	η_w
$\hat{\theta}$	44.7	430.3	-13.5	7.1	0.56
$\hat{\sigma}_\theta$	8.8	20.8	1.3	0.4	0.023
$100\,\hat{\sigma}_\theta / \lvert\hat{\theta}\rvert$	19.7 %	4.8 %	9.6 %	5.6 %	4.1 %

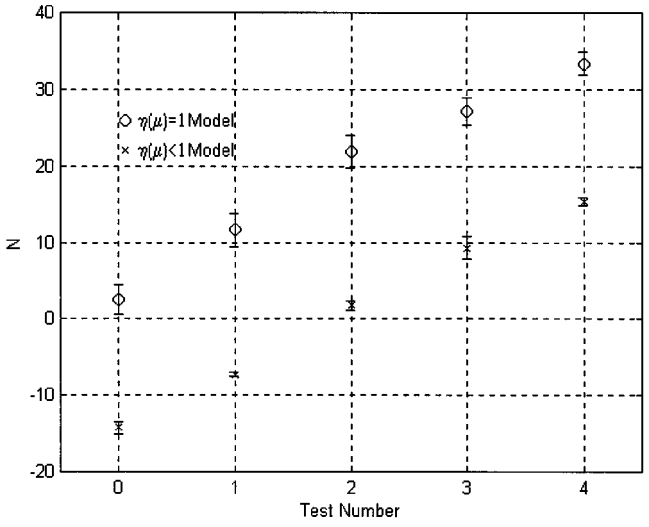

Fig. 6. Buoyancy force estimates with unitary and identified thruster installation coefficient and the corresponding error bars.

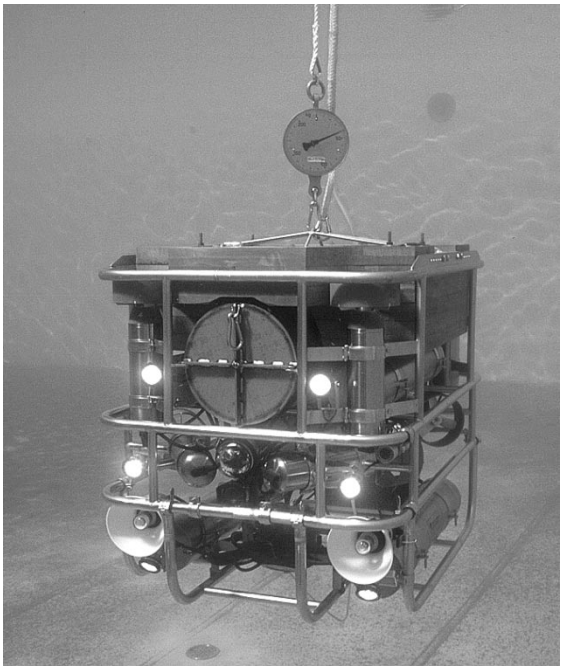

Fig. 7. Static pool test to measure the maximum downward thrust in vertical-all mapping mode.

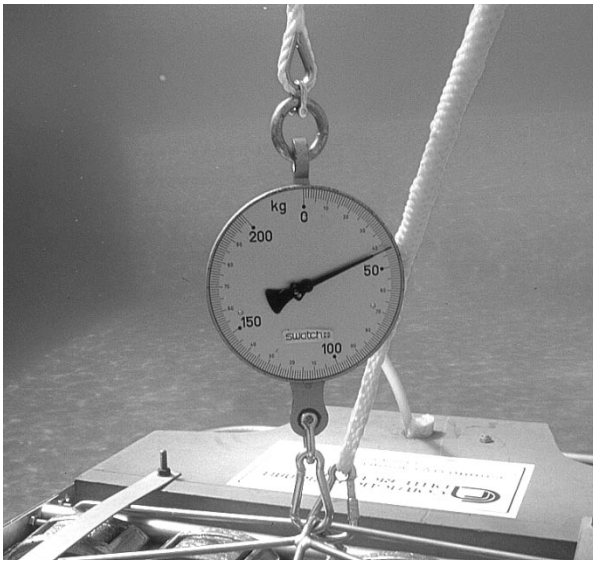

Fig. 8. Zoomed view of the picture reported in Fig. 7 showing the maximum (static) measured downward thrust.

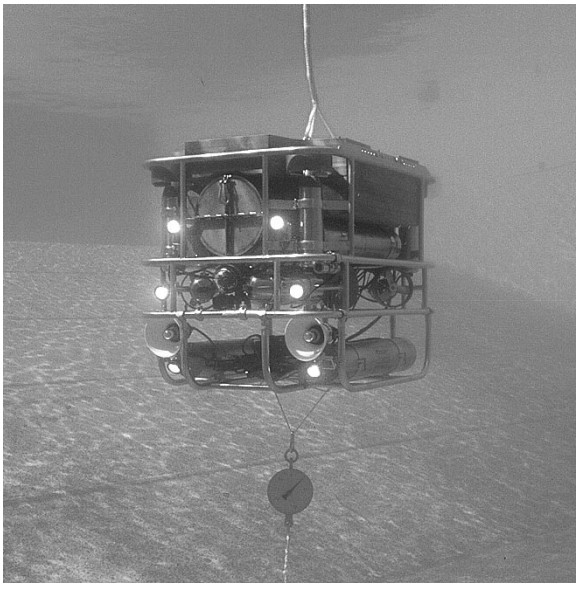

Fig. 9. Static pool test to measure the maximum upward thrust in the vertical-all mapping mode.

The system time constant t_c for the vehicle's yaw motion has been estimated *a priori* to compute the input torque frequency ω_{opt}. The yaw model in the standard yaw rate operating range has been assumed linear, and the yaw inertia identification experiments have been performed by applying the input torque with a thruster mapping having unit efficiency, i.e., the front-left and rear-right thrusters have been used for positive (clockwise) torque and the front-right and rear-left thrusters have been used

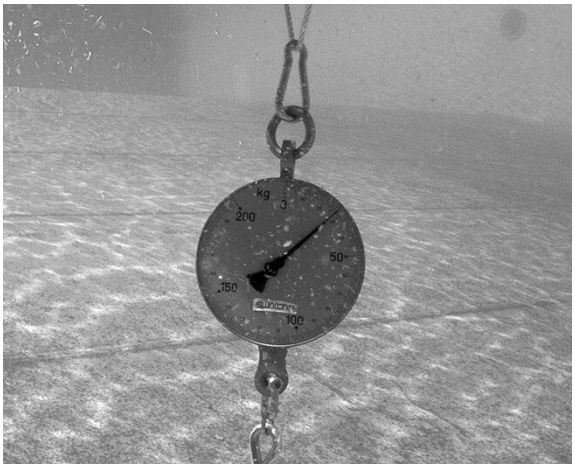

Fig. 10. Zoomed view of the picture reported in Fig. 9 showing the maximum (static) measured upward thrust.

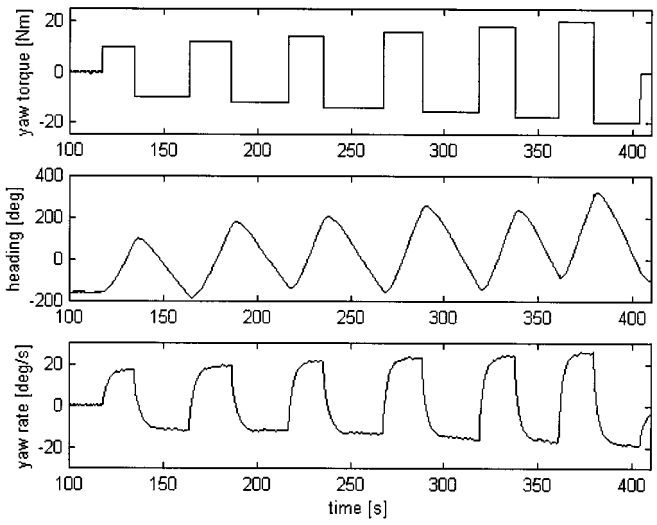

Fig. 11. Top: nominal applied yaw torque (Nm) versus time (s). Middle: relative 10-Hz sampling rate measured heading (deg). Bottom: estimated yaw rate (deg/s) for yaw drag parameter identification.

for negative (counterclockwise) torque. As a consequence, the considered yaw model is

$$I_r \dot{r} = -k_r r + \phi_r \tag{21}$$

where I_r is the ROMEO's z-axis moment of inertia and ϕ_r is the applied torque. The time constant t_c can be estimated *a priori* replacing for I_r the moment of inertia, along its height, of a parallelepiped having a uniformly distributed mass of 450 kg, length 1.3 m, and width 0.9 m, i.e., $I_r = (1/12)450(1.3^2 + 0.9^2) = 93.75$ kg·m^2. The corresponding input frequency, according to (14), is $\omega_{\rm opt} = 0.176$ Hz. During the considered experiment, the input torque was provided by the only rear-left and front-right thrusters, so that unit efficiency is assumed to hold for negative velocity and torque. In accordance with (15), a sinusoidal input torque of amplitude 4 Nm and offset -5 Nm has been applied in order to avoid propeller inversions. The yaw rate was estimated using a symmetric window of 41 points. Implementing the estimation algorithm described in Section III-B yields $\hat{I}_r = (84 \pm 5)$kg·m^2 where the estimation error is computed with the usual technique based on (11) and (12).

The identified model performance is acceptable, as shown in Fig. 12, where the input torque, the filtered yaw rate, and the yaw measurement are reported. In this experiment, assuming the estimated inertia and drag coefficients for the linear model of the vehicle yaw motion, a phase lag between the input torque and the output yaw rate of about 37.5° is expected when an input signal with a period of 24 s is applied. A time lag of 2.6 s is measured, which corresponds to a phase lag of 39°. In Fig. 13, experimental results obtained by applying two sinusoidal torque inputs with offsets of opposite sign are reported. During this experiment, the vehicle worked in the *yaw front-right rear-left* mapping mode, so that propeller–hull interactions reduce the applied torque when it is directed clockwise (positive), as plotted in the top diagram. The measured and estimated, i.e., computed integrating (3), yaw rate are plotted in the bottom diagram, showing an accurate prediction of the vehicle's behavior.

Finally, we consider ROMEO's surge and sway models. During these experiments, the vehicle's heading was kept constant and the position was estimated with respect to a couple of perpendicular walls of the pool. In the case of the surge model, the drag, inertia, and thruster installation parameters have been computed for ROMEO moving both forwards and backwards in the standard and microness toolsled configurations showed in Figs. 1 and 2. To evaluate the loss of efficiency due to propeller–propeller and propeller–hull interactions, the input force has been applied with three different thrust mappings, i.e., *surge front*, *surge rear*, and *horizontal all*. Thrusters are assumed to work in open water when only the front ones push forward and only the rear ones push backward, while propeller–hull interactions are assumed to be present when only the front thrusters push backward or only the rear ones push forward ($\eta_u^{\rm hull} < 1$). When all four thrusters are used, their efficiency is reduced by the combined effects of the propeller–hull and propeller–propeller interactions ($\eta_u^{\rm hull-propeller} < 1$). Different coefficients, denoted by the superscripts $+$ and $-$, have been assumed for the vehicle moving forward and backwards. The vehicle moved at steady-state velocities normally bounded at 0.35 m/s. See Table IV for the estimation results for positive and negative surge motion in the case of technological and microness payload configurations.

Then, experiments for the identification of the vehicle's mass in the surge direction were performed by applying a sinusoidal input force of amplitude 25 N and offset 35 N, corresponding to a regime speed of 0.27 m/s, with only the front thrusters, i.e., assuming the efficiency parameter equal to one. In accordance with (13), the drag coefficient of the linearized system is $k_L = 212.25$(Ns/m). Assuming the inertia $m_u \cong 450 + 50\%(450) = 675$ kg, (13) and (14) suggest an optimal input frequency $\omega_{\rm opt} = 0.18$ Hz. Fig. 14 shows the data relative to the surge inertia identification experiment, where a sinusoidal input of period 26 s has been applied. The input signal frequency is higher than the suboptimal one in order to allow the vehicle to reach the regime speed and to be excited with a couple of sinusoidal periods in a maneuvering space of about 20 m. From top to bottom, the following are displayed: the input force, the 3.3-Hz sampling rate sonar profiler position measurement, and the velocity signal computed using a symmetric window of 21

TABLE III
ROMEO YAW MODEL: ESTIMATED DRAG AND THRUSTER INSTALLATION COEFFICIENTS

		k_r [Nms/rad]	$k_{r\|r\|}$ [Nms^2/rad^2]	η_r^{hull}	$\eta_r^{hull-propeller}$
Linear and quadratic yaw model	$\hat{\theta}$	20.5	49.5	0.60	0.60
	$\hat{\sigma}_\theta$	2.6	7.2	0.03	0.025
	$100\,\hat{\sigma}_\theta/\lvert\hat{\theta}\rvert$	12.7 %	14.5 %	5 %	4.2 %
Linear and quadratic yaw model at low speed	$\hat{\theta}$	23.8	30.8	0.67	0.61
	$\hat{\sigma}_\theta$	3.5	20.7	0.048	0.036
	$100\,\hat{\sigma}_\theta/\lvert\hat{\theta}\rvert$	14.7 %	67.2 %	7.2 %	5.9 %
Linear yaw model at low speed	$\hat{\theta}$	28.6	-	0.68	0.62
	$\hat{\sigma}_\theta$	1.3	-	0.049	0.036
	$100\,\hat{\sigma}_\theta/\lvert\hat{\theta}\rvert$	4.5 %	-	7.2 %	5.8 %

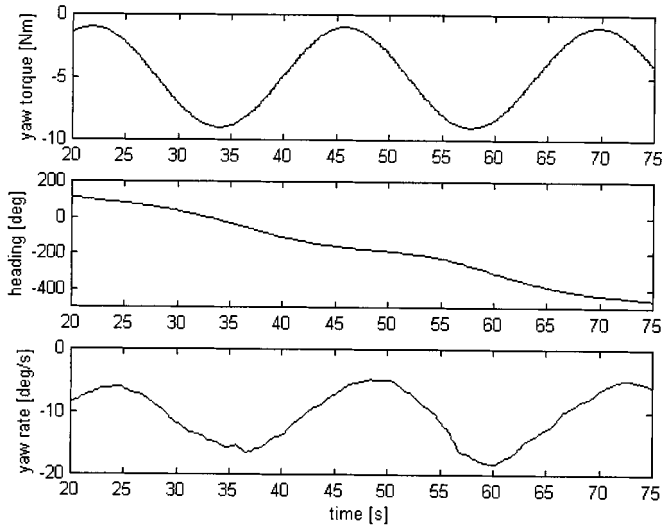

Fig. 12. Top: nominal applied yaw torque (Nm) versus time (s). Middle: relative 10-Hz sampling rate measured heading (deg). Bottom: estimated yaw rate (deg/s) for yaw drag parameter identification.

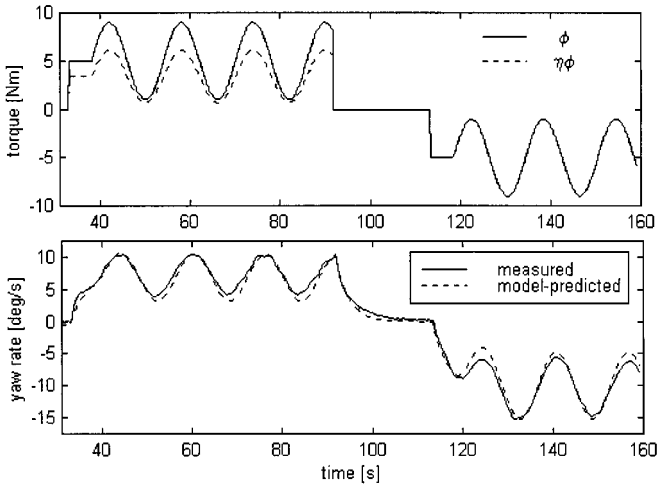

Fig. 13. Yaw model validation. Top: nominal and actual yaw torque (N) versus time (s). Bottom: relative measured and model-predicted yaw rates (deg/s).

points. The solid curves in the position and force plots refer to the data actually adopted for the identification process while the dashed ones show the whole batch of data. Two multipath echoes are visible in the middle of the batch of the sonar measurement data. A mass $\hat{m}_u = (890 \pm 56)$ kg has been estimated, so that a phase lag between the input force and the output surge speed of about $45°$ is expected when an input signal with a period of 26 s is applied. A time lag of 2.7 s is measured (see Fig. 14), which corresponds to a phase lag of $37°$.

Notice that, according to the classical theory of ideal fluids, the surge added mass coefficient of an ellipsoid of total length $2a$, total height $2c$, and total width $2b$ in an ideal fluid of density ρ is given by $\lambda = (4/3)\pi abc\rho h(p, q)$, where $p = a/b$ and $q = c/b$. According to the plots of h reported in [44] and assuming $\rho = 1000$ kg/m^3, the surge added mass coefficient of an ellipsoid having the length, width, and height of ROMEO is $\lambda \approx 183$ kg, i.e., sensibly lower than the estimated value of about 440 kg as $\hat{m}_u \cong 890$ kg, suggesting that the geometry of an open-frame ROV such as ROMEO cannot be successfully approximated by simple shapes.

To evaluate the reliability of the estimated surge model, the speed measurement data of other experiments have been compared with the speed relative to the same input forces predicted according to the model (3). In the top picture of Fig. 15, the applied surge force is plotted (notice that the vehicle worked in surge front mapping mode, i.e., with $\eta_u = 1$), while the measured and estimated surge velocity are shown in the bottom picture.

The sway drag and thruster installation coefficients have been identified analogously. For details, refer to [45].

V. CONCLUSIONS

A procedure for the identification of the drag and inertia parameters of open-frame ROV's and the results of its implementation on a real system have been presented. The identification procedure is based on on-board sensor data rather than towing tank experiments. Although, in principle, towing tank methods allow for a better estimation accuracy (in particular of the inertia coefficients), they are usually performed on a scaled model of the vehicle rather than on the real system [17] with all the related drawbacks. Moreover, such towing tank methods are much

TABLE IV
ROMEO: ESTIMATED DRAG AND THRUSTER INSTALLATION COEFFICIENTS FOR FORWARD AND BACKWARD SURGE MOTION IN TECHNOLOGICAL AND MICRONESS PAYLOAD CONFIGURATION

		k_u^+ [Ns/m]	$k_{u\|u\|}^+$ [Ns^2/m^2]	η_u^{hull+}	$\eta_u^{hull-propeller+}$
forward surge model in technological payload configuration	$\hat{\theta}$	46.9	306.2	0.73	0.73
	$\hat{\sigma}_\theta$	4.9	15.9	0.014	0.014
	$100\hat{\sigma}_\theta/\lvert\hat{\theta}\rvert$	10.4 %	5.2 %	1.9 %	1.9 %
forward surge model in microness payload configuration	$\hat{\theta}$	33.0	326.6	0.72	0.67
	$\hat{\sigma}_\theta$	8.7	27.7	0.024	0.024
	$100\hat{\sigma}_\theta/\lvert\hat{\theta}\rvert$	26.4 %	8.5 %	3.3 %	3.6 %
		k_u^- [Ns/m]	$k_{u\|u\|}^-$ [Ns^2/m^2]	η_u^{hull-}	$\eta_u^{hull-propeller-}$
backward surge model in technological payload configuration	$\hat{\theta}$	57.9	331.4	0.89	0.80
	$\hat{\sigma}_\theta$	5.4	18.9	0.016	0.015
	$100\hat{\sigma}_\theta/\lvert\hat{\theta}\rvert$	9.3 %	5.7 %	1.8 %	1.9 %
backward surge model in microness payload configuration	$\hat{\theta}$	48.4	324.7	0.84	0.63
	$\hat{\sigma}_\theta$	8.3	28.1	0.023	0.023
	$100\hat{\sigma}_\theta/\lvert\hat{\theta}\rvert$	17.1 %	8.7 %	2.7 %	3.7 %

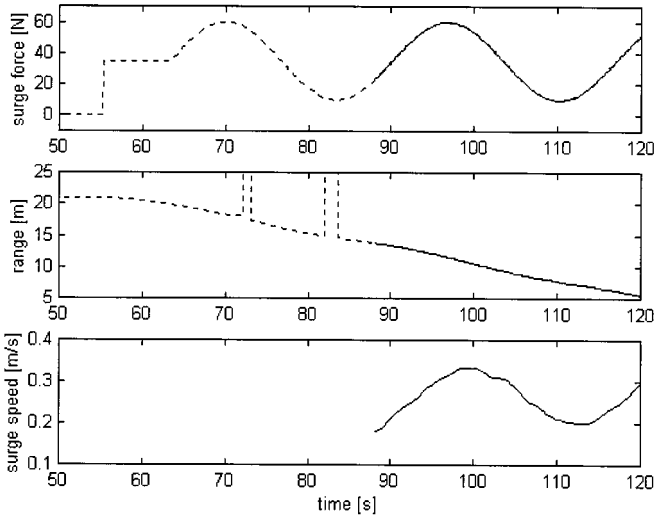

Fig. 14. Surge inertia parameter identification experiments. Top: nominal applied surge force (N) in *surge front* mapping mode versus time (s). Middle: sonar measured position (m) at 3.3-Hz sampling rate. Bottom: estimated velocity (m/s). The dashed lines show the whole batch of data, while the solid ones are relative to the subset of data employed for identification. Two sets of missing sonar measurements are visible between 70–85 s.

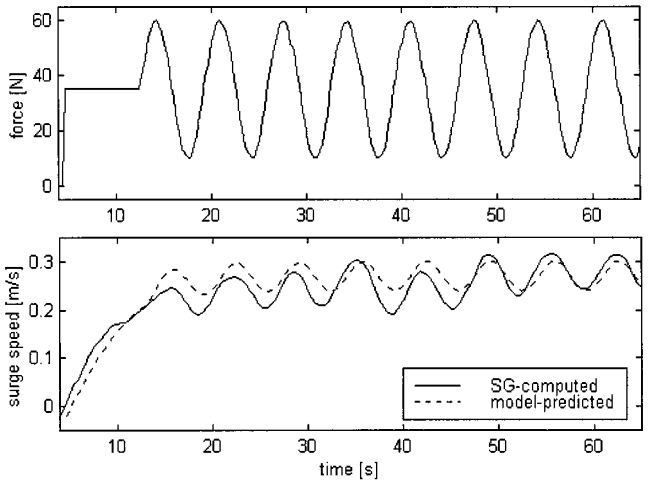

Fig. 15. Surge model validation. Top: nominal applied surge force (N) in *surge front* mapping mode versus time (s). Bottom: relative computed and model-predicted surge velocity (m/s).

more expensive, complex, and time consuming. A simple set of inputs and the relative model fitting technique have been defined for the on-board sensor based estimation of drag, inertia, and thruster installation coefficients of a decoupled lumped parameter ROV model.

The major advantage of the proposed approach consists of the possibility of successfully modeling the propeller–hull and propeller–propeller effects through a thruster installation coefficient that is estimated with the same data adopted for the drag coefficient estimation. Moreover, thanks to their simple nature, the tests may be repeated when the vehicle changes configuration in order to tune the control system when required. It is worth pointing out that the identification procedure has been designed taking into account the vehicle's model structure, the type of available sensors, and the actuator dynamics. Constant velocity tests with different thruster mappings are suggested for the identification of the drag and thruster installation coefficients knowing which sinusoidal input tests are designed for the estimation of the inertia parameters. The developed procedure has been experimentally tested on the surge, sway, heave, and yaw axis of the ROMEO UUV. The data relative to numerous experimental trials and to two payload configurations have been processed and the results are reported in detail. It has been shown that yaw drag in the typical operating yaw rate range, i.e., $|r| \leq 10$ deg/s, is better modeled by a linear term only rather than both a linear and a quadratic one: this is important as it suggests that, as far as the yaw axis is concerned,

linear control techniques may be successfully adopted. It has been shown that the propeller–hull and propeller–propeller interactions may have an extremely important relevance in the dynamics of open-frame ROV's and should thus be taken explicitly into account. Experimental data relative to the ROMEO vehicle show that the thruster's efficiency loss, with respect to the open water thrust tunnel thruster model, due to propeller–propeller and propeller–hull interactions is greater than 10% for each considered axis and reaches the significant value of 44% for heave. Indeed, the proposed identification scheme for the thruster's installation coefficient is simple, low cost, and effective. Finally, it should be noted that the proposed modeling and identification scheme does not necessarily require the thrust tunnel identification of the thrusters. Assuming (6) $\tau = c_V V|V|$ to hold, the vehicle's model (3) can be divided by the unknown c_V and, once a set of suitable thrust mappings with unitary installation coefficients have been heuristically defined on the basis of the vehicle's structure, the whole identification procedure can be implemented adopting the thrusters' input voltage V as the control signal.

ACKNOWLEDGMENT

The authors wish to thank the Robotics Department Staff, R. Bono, G. Bruzzone, G. Bruzzone, and E. Spirandelli, for the support given in ROMEO's hardware and software development, and during the pool tests, and A. Alessandri and Prof. A. Tiano for their contributions in discussions about identification techniques.

REFERENCES

[1] R. D. Ballard, "The MEDEA/JASON remotely operated vehicle system," *Deep-Sea Res.*, vol. 40-8, pp. 1673–1687, 1993.

[2] T. C. Dawe, D. S. Stakes, P. R. McGill, J. Barry, and S. Etchemendy, "Subsea instrument deployments: Methodology and techniques using a work class remotely operated vehicle (ROV)," in *Proc. Oceans'98*, vol. 3, Nice, France, 1998, pp. 1589–1593.

[3] J. B. Newman and D. Stokes, "Tiburon, development of a ROV for ocean science research," in *Proc. Oceans'94*, vol. 2, Brest, France, 1994, pp. 483–488.

[4] W. J. Kirkwood, "Tiburon: Science and technical results from MBARI's new ROV integrated to a SWATH platform," in *Proc. Oceans'98*, vol. 3, Nice, France, 1998, pp. 1578–1583.

[5] M. Nokin, "ROV 6000—A deep teleoperated system for scientific use," in *Proc. 6th IARP Workshop on Underwater Robotics*, Toulon, France, 1996.

[6] ——, "Sea trials of the deep scientific system Victor 6000," in *Proc. Oceans'98*, vol. 3, Nice, France, 1998, pp. 1573–1577.

[7] M. Caccia, R. Bono, G. Bruzzone, and G. Veruggio, "Variable configuration UUV's for marine science applications," *IEEE Robot. Automat. Mag.*, vol. 6, pp. 37–50, June 1999.

[8] A. Terribile, "Advanced ROV package for automatic mobile inspection of sediments (ARAMIS)," in *3rd Eur. Marine Science and Technology Conf.*, vol. IV, Advanced Systems, Lisbon, Portugal, 1998, pp. 1392–1402.

[9] R. Bono, Ga. Bruzzone, Gi. Bruzzone, M. Caccia, E. Spirandelli, and G. Veruggio, "ROMEO goes to Antarctica," in *Proc. Oceans'98*, vol. 3, Nice, France, 1998, pp. 1568–1572.

[10] D. Yoerger and J. J. E. Slotine, "Robust trajectory control of underwater vehicles," *IEEE J. Oceanic Eng.*, vol. OE-10, pp. 462–470, Oct. 1985.

[11] A. J. Healey and D. Lienard, "Multivariable sliding-mode control for autonomous diving and steering of unmanned underwater vehicles," *IEEE J. Oceanic Eng.*, vol. 18, pp. 327–339, July 1993.

[12] D. Fryxell, P. Oliveira, A. Pascoal, C. Silvestre, and I. Kaminer, "Navigation, guidance and control of AUVs: An application to the MARIUS vehicle," *Control Eng. Practice*, vol. 4, no. 3, pp. 401–409, 1996.

[13] G. Conte and A. Serrani, "Robust control of a remotely operated underwater vehicle," *Automatica*, vol. 34, no. 2, pp. 193–198, 1998.

[14] J. Yuh, "Modelling and control of underwater robotic vehicles," *IEEE Trans. Syst., Man, Cybern.*, vol. 20, no. 6, pp. 1475–1483, 1990.

[15] T. I. Fossen and I. E. Fjellstad, "Robust adaptive control of underwater vehicles: A comparative study," in *Proc. 3rd IFAC Workshop on Control Applications in Marine Systems*, Trondheim, Norway, 1995.

[16] K. R. Goheen, "The modelling and control of remotely operated underwater vehicles," Ph.D. dissertation, Univ. of London, 1986.

[17] M. Nomoto and M. Hattori, "A deep ROV 'Dolphin 3K:' Design and performance analysis," *IEEE J. Oceanic Eng.*, vol. OE-11, pp. 373–391, July 1986.

[18] C. Silvestre, A. Aguiar, P. Oliveira, and A. Pascoal, "Control of the SIRENE underwater shuttle: System design and tests at sea," in *Proc. 17th Int. Conf. Offshore Mechanics and Arctic Engineering*, Lisbon, Portugal, 1998.

[19] M. A. Abkowitz, "Measurement of hydrodynamic characteristics from ship maneuvering trials by system identification," *SNAME Trans.*, vol. 80, pp. 283–318, 1980.

[20] G. Liu, "Application of EKF technique to ship resistance measurement," *Automatica*, vol. 29, no. 2, pp. 275–283, 1993.

[21] J. Selkäinaho, "Tuning a dynamic positioning system," *Automatica*, vol. 29, no. 4, pp. 865–875.

[22] T. I. Fossen, S. I. Sagatun, and A. J. Sorensen, "Identification of dynamically positioned ships," *Control Eng. Practice*, vol. 4, no. 3, 1996.

[23] K. R. Goheen and E. R. Jefferys, "The application of alternative modeling techniques to ROV dynamics," in *IEEE Int. Conf. Robotics and Automation, ICRA'90*, Cincinnati, OH, 1990, pp. 1302–1309.

[24] D. B. Marco, A. Martins, and A. J. Healey, "Surge motion parameter identification for the NPS Phoenix AUV," in *IARP—1st Int. Workshop on Autonomous Underwater Vehicles for Shallow Water and Coastal Environment*, Lafayette, IN, 1998, pp. 197–210.

[25] S. Ziani-Cherif, G. Lebret, and M. Perrier, "Identification and control of a submarine vehicle," in *5th IFAC Symp. Robot Control, SYROCO'97*, Nantes, France, 1997, pp. 327–332.

[26] A. Alessandri, M. Caccia, G. Indiveri, and G. Veruggio, "Application of LS and EKF techniques to the identification of underwater vehicles," in *IEEE Int. Conf. Control Applications, CCA'98*, Trieste, Italy, 1998, pp. 1084–1088.

[27] A. T. Morrison III and D. R. Yoerger, "Determination of the hydrodynamic parameters of an underwater vehicle during small scale, nonuniform, 1-dimensional translation," in *Proc. OCEANS'93*, vol. 2, pp. 277–282.

[28] G. Indiveri, "Modelling and identification of underwater robotic systems," Ph.D. dissertation, DIST Univ. of Genova, Italy, 1998.

[29] K. R. Goheen and E. R. Jefferys, "Multivariable self-tuning autopilots for autonomous and remotely operated underwater vehicles," *IEEE J. Oceanic Eng.*, vol. 15, pp. 144–150, July 1990.

[30] J. N. Newman, *Marine Hydrodynamics*. Cambridge, MA: MIT Press, 1977.

[31] T. I. Fossen, *Guidance and Control of Ocean Vehicles*. London, U.K.: Wiley, 1994.

[32] D. Yoerger, J. G. Cooke, and J. E. Slotine, "The influence of thruster dynamics on underwater vehicle behavior and their incorporation into control system design," *IEEE J. Oceanic Eng.*, vol. 15, pp. 167–178, July 1990.

[33] J. Healey, S. M. Rock, S. Cody, D. Miles, and J. P. Brown, "Toward an improved understanding of thruster dynamics for underwater vehicles," *IEEE J. Oceanic Eng.*, vol. 20, pp. 354–361, Oct. 1995.

[34] C. L. Tsukamoto, W. Lee, J. Yuh, S. K. Choi, and J. Lorentz, "Comparison study on advanced thruster control of underwater robots," in *IEEE Int. Conf. Robotics and Automation, ICRA'97*, 1997, pp. 1845–1850.

[35] L. L. Whitcomb and D. R. Yoerger, "Comparative experiments in the dynamics and model-based control of marine thrusters," in *Proc. IEEE/MTS OCEANS'95*, vol. 2, pp. 1019–1028.

[36] J. Yuh, "Learning control for underwater robotic vehicles," *IEEE Contr. Syst. Technol.*, pp. 39–46, April 1994.

[37] C. G. Goodwin and R. L. Payne, *Dynamic System Identification: Experiment Design and Data Analysis*, New York: Academic, 1977.

[38] L. Ljung, *System Identification Theory for the User*. Englewood Cliffs, NJ: Prentice-Hall, 1987.

[39] J. Swevers, C. Ganseman, B. D. Tükel, J. De Schutter, and H. Van Brussel, "Optimal robot excitation and identification," *IEEE Trans. Robot. Automat.*, vol. 13, pp. 730–740, May 1997.

[40] J. Swevers and C. Ganseman, "Experimental identification of robot manipulators," in *Proc. Workshop Modeling and Control of Mechanical Systems*, London, U.K., 1997, pp. 137–152.

[41] W. H. Press, S. A. Teukolsky, W. T. Vetterling, and B. P. Flannery, *Numerical Recipes in C*. Cambridge, U.K.: Cambridge Univ. Press, 1992.
[42] A. Alessandri, R. Bono, M. Caccia, G. Indiveri, and G. Veruggio, "Experiences on the modelling and identification of the heave motion of an open-frame UUV," in *Proc. Oceans '98*, vol. 2, Nice, France, 1998, pp. 1049–1053.
[43] Y. Bar-Shalom and X. R. Li, *Estimation and Tracking: Principles, Techniques, and Software*. Boston, MA: Artech House, 1993.
[44] N. E. Kochin, I. A. Kibel, and N. V. Roze, *Theoretical Hydromechanics*: Interscience Publisher, 1964.
[45] M. Caccia and G. Indiveri, "Identification of the ROMEO's sway drag and thruster installation coefficients,", C.N.R.–I.A.N. Tech. Rep. 346/99, 1999.

Massimo Caccia (M'96) was born in 1966. He received the Laurea degree in electronic engineering from Genoa University, Italy, in 1991.

That same year, he received a Post-Graduate Research Grant from Ansaldo, a leading Italian industrial engineering company, to study sonar-based motion planning and control in wheeled land vehicles. In 1993, he collaborated with the Telerobot Consortium, focusing on real-time control architectures and afterward joined the Istituto Automazione Navale (IAN) in Genoa, as a Research Scientist. His research at IAN has encompassed numerous subjects, notably software architectures for intelligent underwater vehicles, sensor-based navigation, guidance, and control, modeling, identification, and simulation of unmanned underwater vehicles, and in-water testing. He participated in the XIII Italian Expedition to Antarctica in 1997–1998 working on under-ice performance evaluation of acoustic devices for underwater vehicles.

Giovanni Indiveri was born in 1970. He received the Laurea degree in physics and the Ph.D. degree in electronic engineering and computer science, both from Genoa University, Genoa, Italy, in 1995 and 1999, respectively. His Ph.D. research, on modeling and identification of underwater robotic systems, was funded by the Italian National Research Council and was carried out at the Istituto Automazione Navale (IAN), in Genoa.

He is currently employed at the Institute for Intelligent Autonomous Systems AiS of GMD, the German National Research Center for Information Technology, St. Augustin, Germany, as a Post-Doctoral Researcher in autonomous underwater robotics. His research interests focus on dynamic modeling and control and path planning of underwater vehicles.

Gianmarco Veruggio received the Laurea degree in electronic engineering from Genoa University, Italy, in 1980.

He is currently Head of the Marine Robotics Department at Istituto per l'Automazione, Navale (IAN), National Research Council, Genoa, Italy. From 1980 to 1983, he was with the Automation Division of Ansaldo, a leading Italian industrial engineering company, as a designer of fault-tolerant multi-processor architectures for fail-safe control systems. In 1984, he joined IAN as a Computer Scientist. He has worked on real-time computer graphics for simulation, control techniques, and naval and marine data collection systems. He was the Leader of experimental campaigns on-board Italian oceanographic ships. He is a Task Leader in the AMADEUS and ARAMIS Projects, both funded by the European Community under the MAST Programme. He led the first underwater robotics campaign in Antarctica during the IX Italian Expedition in 1993–1994, as well as the following XIII Expedition in 1997–1998 for the exploitation of the Romeo prototype. His research interests encompass mission control in AUV's, real-time man-machine interfaces, and control systems for tele-operation.

Mr. Veruggio is a member of the IEEE Oceanic Engineering Society.